

# ***hMSH2* expression is associated with paclitaxel resistance in ovarian carcinoma, and inhibition of *hMSH2* expression *in vitro* restores paclitaxel sensitivity**

JIN ZHANG<sup>1</sup>, DONGMEI YIN<sup>2</sup> and HONGXIA LI<sup>1</sup>

<sup>1</sup>Department of Obstetrics and Gynecology, Beijing Shijitan Hospital, Capital Medical University, Haidian, Beijing 100038; <sup>2</sup>Department of Gynecology, Beijing Obstetrics and Gynecology Hospital, Capital Medical University, Dongcheng, Beijing 100006, P.R. China

Received May 19, 2014; Accepted July 25, 2014

DOI: 10.3892/or.2014.3430

**Abstract.** The objective of the present study was to investigate the association between paclitaxel resistance, gene copy number, and gene expression in ovarian carcinoma, and to restore paclitaxel sensitivity in a paclitaxel-resistant ovarian carcinoma cell line by using *hMSH2*-targeting siRNA. Paclitaxel-resistant ovarian carcinoma cell lines OC3/TAX300 and OC3/TAX50 and their parental cell lines were analyzed by comparative genomic hybridization, and the expression levels of *hMSH2* in ovarian carcinoma cell lines and tissues were determined. An siRNA targeted to *hMSH2* mRNA was used to transfect a paclitaxel-resistant cell line. We assessed the morphological features, proliferation, and susceptibility to apoptosis of the transfected cells after paclitaxel treatment. Chromosome 2p21 (gene locus of *hMSH2*) was amplified in OC3/TAX300 cells. *hMSH2* was overexpressed in 93.9 and 47.6% of paclitaxel-treated and untreated ovarian carcinoma tissue samples ( $P=0.0001$ ), respectively. *hMSH2* was overexpressed in 93.3 and 54.2% of low-differentiated and moderate-to-highly differentiated ovarian carcinoma tissue samples ( $P=0.0008$ ), respectively. *hMSH2* expression was inhibited in the OC3/TAX300 cells transfected with *hMSH2* siRNA. *hMSH2* siRNA increased paclitaxel sensitivity, inhibited OC3/TAX300 cell proliferation (G<sub>2</sub>/M arrest), and increased susceptibility to apoptosis. *hMSH2* expression was upregulated in ovarian carcinoma cell lines and tissues after paclitaxel treatment. *hMSH2* overexpression is related to paclitaxel resistance and poor prognosis. Inhibition of *hMSH2* expression *in vitro* restores paclitaxel sensitivity in

paclitaxel-resistant ovarian carcinoma cell lines and indicates a new direction in adjuvant therapy for ovarian carcinoma.

## **Introduction**

The death rate of patients with ovarian carcinoma is one of the highest for gynecologic malignancies (1). Paclitaxel plus platinum therapy is gaining acceptance as the standard clinical chemotherapy regimen for ovarian cancer. Paclitaxel is an important new agent for ovarian cancer treatment and is highly effective as the first-line therapy for advanced ovarian cancer. However, the emergence of a paclitaxel-resistant tumor subpopulation ultimately leads to treatment failure. Therefore, determining the mechanism underlying paclitaxel resistance is important.

Comparative genomic hybridization (CGH) detects the chromosomal loci DNA copy-number changes in a single experiment. CGH analyses of ovarian cancer cell lines resistant to paclitaxel and platinum revealed that they harbor drug resistance-related chromosomal abnormalities (2,3). For example, the increased DNA copy-number at 6q21-25 and decreased DNA copy-number at 7q21-36 and 10q12-15, respectively, are associated with platinum resistance, and the increased DNA copy-number at 7q11.2-21 is related to paclitaxel resistance (3). In the present study, we conducted CGH analyses to compare the genomic alteration present in paclitaxel-resistant ovarian carcinoma cell lines with those present in their parental cell lines. These analyses revealed high amplification of chromosome 2p21 in paclitaxel-resistant OC3/TAX300 cells. Certain drug resistance-related genes are located on chromosome 2p21, including *hMSH2*, a member of the mismatch repair (MMR) gene family. MMR, which corrects base mismatch, ensures DNA replication fidelity, and maintains genomic stability.

In human cells, the mechanism of MMR mainly includes three processes: mismatch identification, mismatch excision, and DNA resynthesis. MMR involves hMSH1, hMSH2, hMSH6, PMS1, and PMS2 proteins (4,5). The dysfunction of MMR, which causes the failure of mismatch base repair, will induce the genomic instability caused by the increased frequency of spontaneous mutations, leading to tumorigenesis. Studies have shown that MMR dysfunction (most frequently

---

*Correspondence to:* Professor Hongxia Li, Department of Obstetrics and Gynecology, Beijing Shijitan Hospital of Capital Medical University, 10 Tieyi Road, Haidian, Beijing 100038, P.R. China  
E-mail: lihx6260@gmail.com

**Key words:** comparative genomic hybridization, *hMSH2*, ovarian carcinoma, paclitaxel resistance, siRNA

*hMSH1* or *hMSH2*) is an important genetic risk factor for hereditary nonpolyposis colorectal cancer, which is also called Lynch syndrome (6). Lynch syndrome is a hereditary syndrome related to some familial cancers, such as colorectal cancer, as well as extracolonic cancers such as endometrial, gastric, ovarian, pancreatic, ureteral, and brain cancers, and sebaceous adenomas (6-8). Deficiency of MMR proteins leads to an accumulation of DNA replication errors and allows the persistence of mismatch mutations, particularly in areas of the genome with short repetitive DNA known as 'microsatellites'; this phenomenon is known as microsatellite instability (MSI) (9). More than 90% of colorectal cancers related to Lynch syndrome manifest MSI. MSI is also associated with 15-20% of sporadic colorectal cancers (10-12).

However, if *hMSH2* is overexpressed in tumor cells, the DNA damage in these cells can be repaired rapidly, leading to tumor progression, deterioration and chemotherapy resistance, ultimately resulting in poor prognosis (4,13). For decades, studies have confirmed that an increase in the ability of cells to repair damaged DNA is a crucial factor in determining the resistance elicited against DNA-damaging agents such as alkylating agents and platinum-based compounds (13-16).

Paclitaxel, the most common chemotherapeutic drug in ovarian cancer treatment, can generate free radicals leading to irreversible oxidative DNA damage (17). Therefore, we designed the present study to investigate the relationship between *hMSH2* and paclitaxel resistance. In previous studies, we established the paclitaxel-resistant ovarian carcinoma cell lines OC3/TAX300 and OC3/TAX50 by exposing OC3 ovarian carcinoma cells to various doses of paclitaxel (18). The resistance index (RI) of OC3/TAX300 and OC3/TAX50 cell lines is 6.70 and 2.52, respectively. In the present study, we analyzed *hMSH2* expression among different ovarian cancer cell lines and tissues. We employed siRNA techniques to assess the morphological features, proliferation, and apoptosis susceptibility in the paclitaxel-resistant OC3/TAX300 cell line.

## Materials and methods

**Ethics statement.** The study was approved by the Ethics Committee of the Beijing Shijitan Hospital of Capital Medical University. Written informed consent was obtained from all the patients and families before surgery. All procedures were performed in accordance with the Declaration of Helsinki.

**Cell lines and culture conditions.** The OC3 human ovarian carcinoma cell line was provided by the Basic Medical Research Institute (Beijing, China) and was used in several studies (19). The paclitaxel-resistant ovarian carcinoma cell lines OC3/TAX300 and OC3/TAX50 were established in previous studies (18). Cells were cultured in RPMI-1640 medium (Gibco, Carlsbad, CA, USA) supplemented with 10% bovine calf serum (DingGuo Co. Ltd., Beijing, China), and 0.1% each of penicillin and streptomycin at 37°C in an incubator with a 5% CO<sub>2</sub> atmosphere.

**Reagents and antibodies.** Rabbit anti-human *hMSH2* monoclonal antibody was purchased from Cell Signaling Technology Co. (Boston, MA, USA). TRIZOL<sup>®</sup> reagent kit and Lipofectamine<sup>®</sup> were supplied by Invitrogen (Life Technologies

Co., Carlsbad, CA, USA). Dimethyl sulfoxide (DMSO) was purchased from Sigma-Aldrich (St. Louis, MO, USA). The Annexin V-PE/7-AAD (7-amino-actinomycin D) apoptosis test kit was from Kaiji Technology Co. Ltd. (Nanjing, China). Paclitaxel was purchased from ChenXin Medicine Co. Ltd. (Jining, China). Phosphate-buffered saline, propidium iodide, 3-(4,5-dimethylthiazol-2-yl)-2,5-diphenyl tetrazolium bromide (MTT), and microplates were purchased from DingGuo Co. Ltd.

**Clinical samples.** We collected 54 ovarian cancer tissue samples (preserved in liquid nitrogen) from the specimen repository of Beijing Shijitan Hospital from March 2008 to May 2013. The tissue samples were divided into 2 sets as follows: 33 tissue samples with paclitaxel chemotherapy before surgery and 21 without paclitaxel chemotherapy before surgery; 30 samples with low-differentiated ovarian carcinoma tissue and 24 with moderate-to-highly differentiated ovarian carcinoma tissue.

**Comparative genomic hybridization (CGH).** Genomic DNA was extracted from the paclitaxel-resistant cell lines, OC3/TAX300 and OC3/TAX50, the paclitaxel-sensitive cell line OC3, and the peripheral blood of healthy women volunteers using the standard phenol/chloroform method. OC3/TAX300, OC3/TAX50 and OC3 DNA were labeled with fluorescein-dUTP (green fluorescence). DNA from normal peripheral blood was labeled with rhodamine-dUTP (red fluorescence) using a nick-translation method. Metaphase chromosome spreads prepared from the lymphocytes of the healthy women were hybridized with a sample DNA probe or a matched normal peripheral-blood DNA probe, respectively. The differential fluorescence of chromosomes was observed using a fluorescence microscope. The fluorescence intensity, fluorescence ratio, and analysis diagrams were compared using a fluorescence image analysis system.

**Reverse transcription-polymerase chain reaction (RT-PCR) assay.** The *hMSH2* primers, designed and synthesized by Shengong Co. Ltd., (Shanghai, China) were: forward, 5'-CAA TTG AAA GGA GTC TCC ACG-3' [21 base pairs (bp)]; and reverse, 5'-AAA CTC CTC AAG TTC CAG GG-3' (20 bp). The length of the amplified DNA fragment was 411 bp. RNA was extracted using the TRIZOL reagent kit. The PCR reaction mixture (20  $\mu$ l total volume) composition was as follows: 2  $\mu$ l 10X PCR buffer, 1.5  $\mu$ l 10 mmol/l deoxynucleoside triphosphate (dNTP), 2.4  $\mu$ l MgCl<sub>2</sub> (25 mmol/l), 2  $\mu$ l each forward and reverse primer, 1  $\mu$ l cDNA, 0.1  $\mu$ l Taq DNA polymerase, and 9  $\mu$ l distilled water. The PCR reaction conditions were as follows: denaturation at 94°C for 5 min; 35 cycles each of denaturation at 95°C for 50 sec, annealing at 55°C for 1 min, and extension at 72°C for 2 min; followed by a final extension at 72°C for 7 min. A 10- $\mu$ l sample of each reaction was subjected to electrophoresis on a 2% agarose gel, and the gel was stained with ethidium bromide after electrophoresis for DNA band visualization.

**Transfection with siRNA.** The small interfering RNA (siRNA) oligonucleotides were synthesized by Jikai Gene Chemical Technology Co. Ltd. (Shanghai, China). According to the

principles of siRNA design using the RNA online tools of Invitrogen and the mRNA sequences of *hMSH2* in GenBank (Gene ID: 4436), 3 siRNA targeting different parts of *hMSH2* mRNA and an siRNA with a random sequence were designed (*hMSH2*-siRNA-#1, *hMSH2*-siRNA-#2, *hMSH2*-siRNA-#3 and negative-siRNA; Table I). The BLAST sequence alignment algorithm was used to exclude homology (<http://blast.ncbi.nlm.nih.gov/Blast.cgi>) (20).

We constructed pGCSIL-GFP-*hMSH2* and pGCSIL-GFP-negative lentivirus vectors. 293T cells were cotransfected with plasmid pGCSIL-GFP, pHelper1.0, and pHelper2.0 to produce a virus stock (Genechem Co. Ltd., Shanghai, China). The OC3/TAX300 ovarian carcinoma cell line was subjected to 3 types of treatments (groups): i) experimental (EX) groups, in which cells were transfected with the *hMSH2*-siRNA-1#-plasmid, *hMSH2*-siRNA-2#-plasmid, and *hMSH2*-siRNA-3#-plasmid; the titer of the virus was  $2 \times 10^9$ ,  $4 \times 10^8$  and  $3 \times 10^8$  TU/ml, respectively; ii) negative control (NC) group, in which cells were transfected using a negative-siRNA-plasmid that has been used as the negative control in a number of studies (21,22), and has only 16 consecutive bases that are identical to 2 genes in zebrafish among all sequences in the GenBank database; iii) blank control (BC) group, in which cells were not transfected.

The OC3/TAX300 ovarian carcinoma cell line was cultured in RPMI-1640 medium supplemented with 10% bovine calf serum at 37°C in an incubator with a 5% CO<sub>2</sub> atmosphere and passaged every 2 days. When the cells reached the logarithmic growth phase, they were added to the wells of a 96-well plate at a concentration of  $3.0\text{--}5.0 \times 10^4$  cells/ml ( $90 \mu\text{l/well}$ ). When the cells were 70–80% confluent, they were transfected in the presence of Lipofectamine 2000 (LF2000, Invitrogen), according to the manufacturer's protocol. Transfection efficiency was determined 72 h after transfection, by measuring the green fluorescence intensity of the cells in each well by fluorescence microscopy. Transfection efficiency was determined using the formula: Transfection efficiency (%) = (the number of fluorescent cells/the total number of cells) x 100%. A cell line with better transfection efficiency was used for subsequent experiments. All experiments were performed in triplicate.

**Real time-PCR analysis.** Total RNA was extracted from the cultured cells using TRIzol reagent. *hMSH2* primers were designed according to sequence data obtained from GenBank, and *ACTB* ( $\beta$ -actin) was used as an internal control. The primer sequences were as follows: 5'-AAG AAG CCC AGG ATG CCA TT-3' (sense) and 5'-AGC ATC TAG CTG AGC TAA CAC ATC A-3' (antisense) for *hMSH2*; 5'-AGG TCA TCA CCA TTG GCA ATG-3' (sense) and 5'-GGT AGT TTC GTG GAT GCC ACA-3' (antisense) for *ACTB*. Real time-PCR cycling parameters were as follows: 50°C for 2 min; 95°C for 10 min; and 40 cycles each of 95°C for 15 sec and 60°C for 1 min for the amplification curve and 95°C for 15 sec, 60°C for 15 sec, and 95°C for 15 sec for the dissociation curve. The data were analyzed using SDS 2.2 software and exported to an Excel spreadsheet. Target gene expression was normalized to that of *ACTB*. The mRNA expression ratio of *hMSH2/ACTB* was calculated using  $2^{-\Delta\Delta Ct}$  analysis, which represents the relative expression values of *hMSH2* mRNA. Ct is the number of cycles when the DNA concentration reached the threshold.

Table I. siRNA sequences.

Genes	Sequence
<i>hMSH2</i> -siRNA-#1	CTTGCTGAATAAGTGTAATA
<i>hMSH2</i> -siRNA-#2	TGGCAATCTCTCTCAGTTT
<i>hMSH2</i> -siRNA-#3	AGTAATGGAATGAAGGTAA
Negative-siRNA	TTCTCCGAACGTGTACCGT

The formula is as follows:  $\Delta Ct = Ct(hMSH2) - Ct(ACTB)$ .  $\Delta\Delta Ct = \Delta Ct(\text{experimental group}) - \Delta Ct(\text{blank control})$ .

**Western blot analysis.** The transfected cells were centrifuged at 4°C (5,000 rpm, 5 min) and the supernatant was saved. Total cell lysates were prepared using cell-lysis buffer. After the cell lysates were incubated for 30 min on ice, they were centrifuged at 4°C (12,000 rpm, 10 min) and heated at 100°C for 5 min. The extracted proteins (30–40  $\mu\text{l}$ ) were separated using 10% sodium dodecylsulfate-polyacrylamide gel electrophoresis (SDS-PAGE) and were electrophoretically transferred onto an Immobilon-P membrane. The membranes were incubated in a blocking solution for 1–3 h at room temperature and then incubated with rabbit anti-human *hMSH2* monoclonal antibodies (diluted 1:1,000) at 4°C overnight. After the membranes were washed three times with Tris-buffered saline with Tween-20, they were incubated for 1–2 h with a fluorescent secondary antibody (diluted 1:5,000) at room temperature. The membranes were washed as described above and analyzed using a two-color infrared imaging system (Odyssey; Li-COR, Lincoln, NE, USA). The gray level of each band was calculated using the image processing software Image J (National Institutes of Health, Bethesda, MD, USA).

**MTT assay.** The IC<sub>50</sub> value of paclitaxel was determined in each of the 3 groups. Cells in the logarithmic growth phase were seeded into 96-well plates at a concentration of  $1 \times 10^4$  cells/well. On reaching confluency, the cells were treated with paclitaxel at various concentrations: 0 (control), 1, 2, 4, 8, 16 and 32  $\mu\text{g/ml}$  for 48 h. IC<sub>50</sub> of paclitaxel was determined in triplicate for each group. The cells were incubated at 37°C in an incubator with a 5% CO<sub>2</sub> atmosphere. At the end of the treatment, the medium was removed by vacuum and replaced with 200  $\mu\text{l}$  of fresh RPMI-1640 medium. Twenty microliters of MTT stock solution (5 mg/ml) was added to each well after which the cells were incubated for an additional 4 h. The supernatant was then removed and cell pellets were resuspended in 150  $\mu\text{l}$  DMSO by using 5 min of constant agitation. Cell viability was determined by measuring the absorbance at 492 nm using a microplate reader. The following equation was used to calculate cell growth inhibition rate: Cell growth inhibition rate = [1 - (absorbance value of each well treated with paclitaxel/absorbance value of the control well without paclitaxel)] x 100%. IC<sub>50</sub> of paclitaxel was measured by chartography.

**Flow cytometric analysis of apoptosis and the cell cycle.** Cells in logarithmic phase were treated with 2  $\mu\text{g/ml}$  of paclitaxel for 24 and 48 h. After the culture media was removed, the cells were trypsinized (0.25% trypsin without EDTA), washed twice

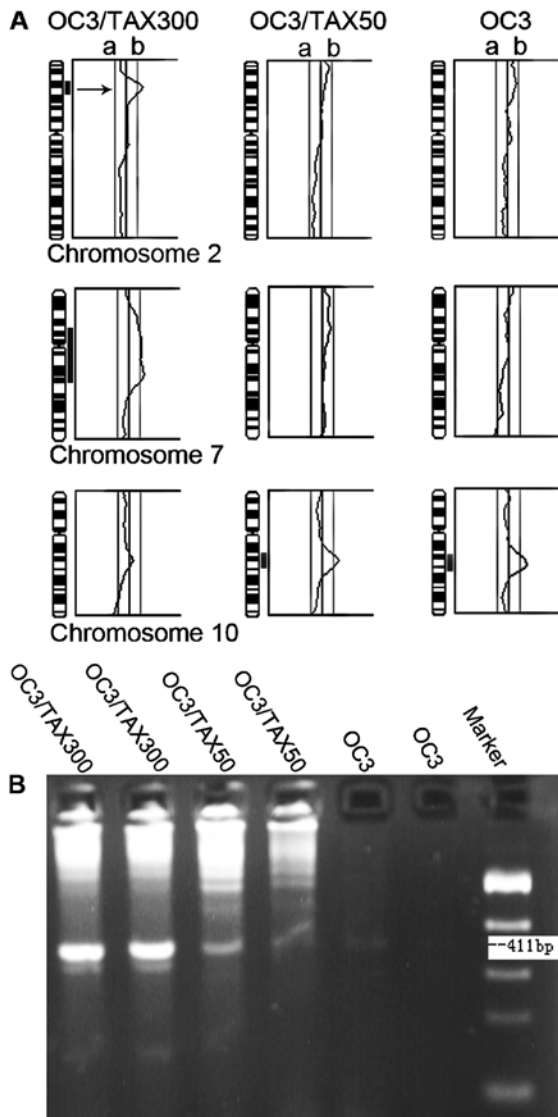


Figure 1. CGH and RT-PCR analysis of *hMSH2* expression in ovarian carcinoma cell lines. (A) Chromosome 2p21 amplification was only detected in OC3/TAX300 cells. Loss of chromosomes 7q was only detected in OC3 cells. Amplification of chromosome 10q22 was detected in OC3 and OC3/Tax50 cells. The left of line 'a' indicates loss of chromosomes; the right of line 'b' indicates amplification of chromosomes. (B) *hMSH2* was overexpressed by OC3/TAX300 cells, weakly expressed by OC3/TAX50, and not detectably expressed by OC3 cells.

with phosphate-buffered saline, and made into a single-cell suspension at a concentration of  $1.5 \times 10^6$  cells/ml. Next, 1 ml of the cell suspension was centrifuged at 200 rcf for 10 min at 4°C, and the pellet was resuspended in 500  $\mu$ l flow cytometry binding buffer. In accordance with the instructions of the Annexin V-PE/7-AAD apoptosis test kit, 20  $\mu$ l propidium iodide was added to the suspension, and the tube was incubated at room temperature for 1 h in the dark. Flow cytometric analysis was then performed to determine cell viability and to analyze the progression of the cell cycle after the treatment.

*Electron microscopic observations of apoptosis-induced morphological changes.* Cells in each of the 3 groups were treated with 2  $\mu$ g/ml paclitaxel for 48 h and fixed in 4% glutaraldehyde at 4°C for 1.5 h. The cells were rinsed with rinse solution (0.18 M sucrose in 0.1 MPB, 4°C) twice and further

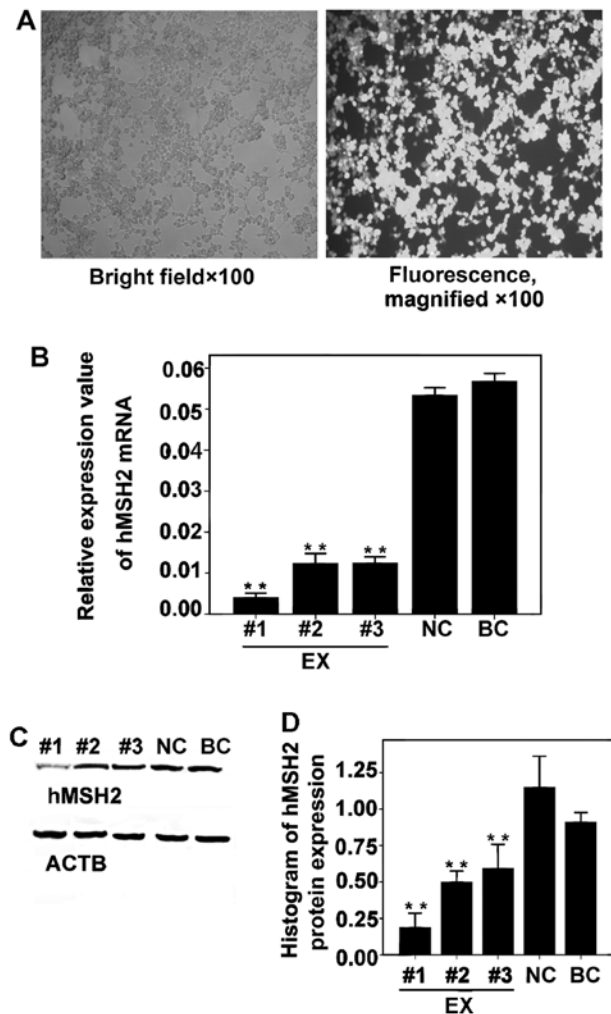


Figure 2. Effect of *hMSH2*-siRNA on *hMSH2* mRNA and protein expression in OC3/TAX300 cells. (A) siRNA transfection efficiency. (B) Relative expression levels of *hMSH2* mRNA in the EX groups were significantly reduced. (C and D) Protein expression of *hMSH2* in the EX groups was significantly inhibited. EX, experimental groups; #1, *hMSH2*-siRNA-#1 group; #2, *hMSH2*-siRNA-#2 group; #3, *hMSH2*-siRNA-#3 group; NC, negative control group; BC, blank control group.

incubated with osmium tetroxide for 1 h. Cells were then washed in distilled water, dehydrated with graded ethanol, and embedded in solidifying medium for ultra-thin sectioning. The sections were dyed with uranyl acetate and lead citrate. Typical ultrastructural changes in cell apoptosis were visualized under transmission electron microscopy.

*Statistical analysis.* Statistical analysis was performed using SPSS software (version 17.0 for Windows). Data are presented as mean values  $\pm$  standard deviation (SD) and comparisons were performed using a t-test.  $P \leq 0.05$  was considered to indicate a statistically significant difference.

**Results**

*CGH and RT-PCR analysis show hMSH2 overexpression in paclitaxel-resistant ovarian carcinoma cells.* CGH analysis revealed extensive genomic alterations in all 3 cell lines (Fig. 1A). Chromosome 2p21 amplification was detected only in the OC3/TAX300 cells. The PCR results correlated

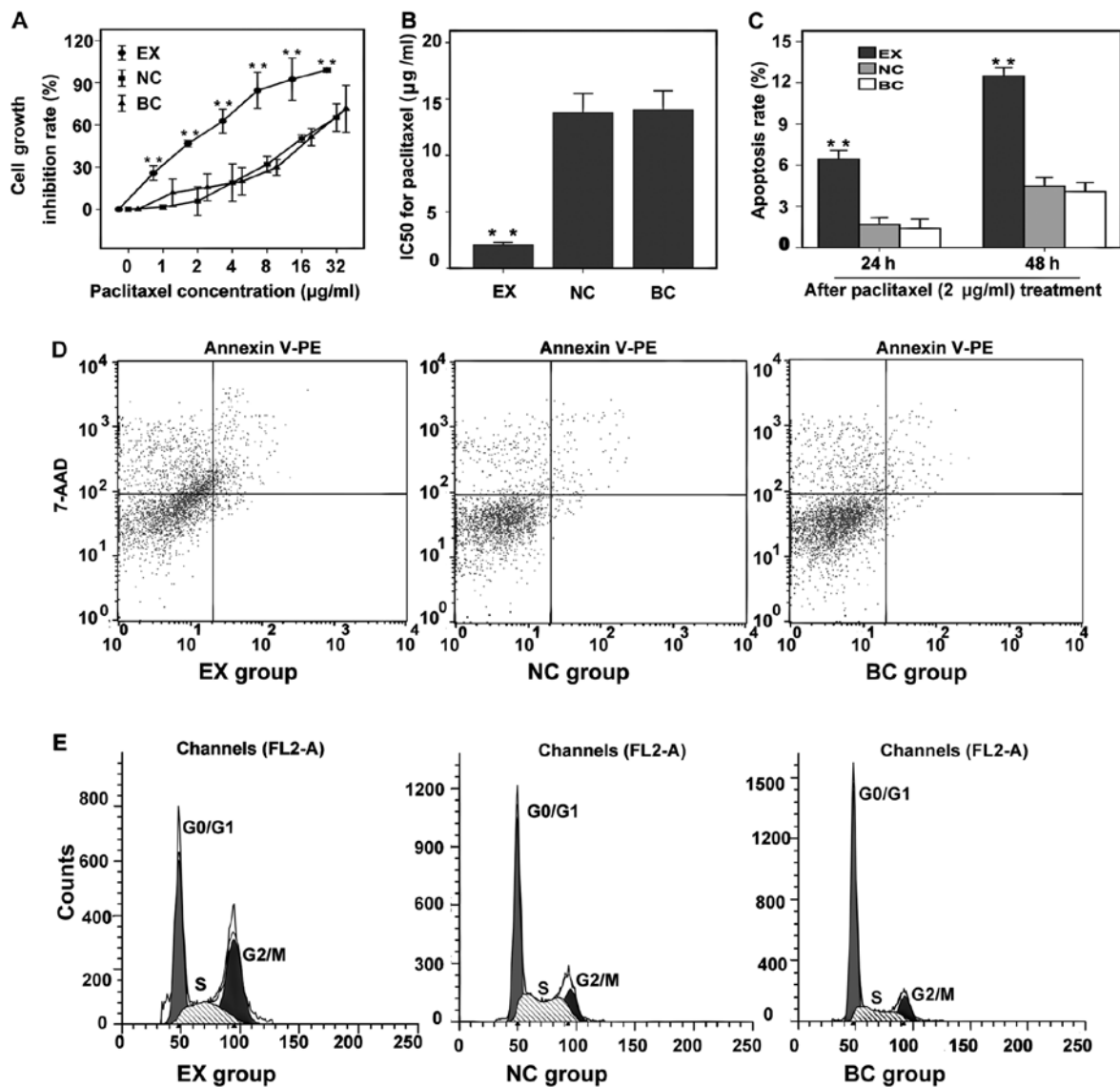


Figure 3. Effect of the inhibition of *hMSH2* expression on paclitaxel resistance. (A) Cell growth inhibition rate curves of cells in all groups after paclitaxel treatment in the following concentration gradient: 0, 1, 2, 4, 8, 16 and 32  $\mu\text{g/ml}$ . (B) The  $\text{IC}_{50}$  for paclitaxel in the 3 groups. (C) Apoptosis rate at 24 and 48 h after paclitaxel (2  $\mu\text{g/ml}$ ) treatment (%). (D) Apoptosis rate at 48 h after paclitaxel treatment (%). Lower left quadrant, living cells; lower right quadrant, early apoptotic cells; upper right quadrant, late apoptotic cells; upper left quadrant, necrotic cells. Apoptosis rate = number of apoptotic cells/total cells  $\times$  100%. (E) Cell cycle analysis at 48 h after paclitaxel (2  $\mu\text{g/ml}$ ) treatment. EX group, experiment group; NC group, negative control group; BC group, blank control group.

closely with the CGH results, which revealed chromosome 2p21 (gene locus of *hMSH2*) amplification (Fig. 1B). The expression rates of paclitaxel-treated and paclitaxel-untreated tissue samples were 93.9 (31/33) and 47.6% (10/21), respectively ( $P=0.0001$ ). The expression rate was 93.3 and 54.2% in low-differentiated ovarian carcinoma tissue samples and moderate-to-highly differentiated tissue samples, respectively ( $P=0.0008$ ).

*hMSH2*-siRNA inhibits *hMSH2* mRNA and protein expression in OC3/TAX300 cells. We found that the cells were transfected at the highest efficiency and that almost all cells emitted green fluorescence (Fig. 2A). The relative expression levels of *hMSH2* mRNA in the EX groups were significantly reduced, particularly by *hMSH2*-siRNA-#1 in comparison with the results of the NC ( $P<0.001$ ) and BC groups ( $P<0.001$ ; Fig. 2B). *hMSH2* protein expression in the EX group was significantly

inhibited, particularly by *hMSH2*-siRNA-#1, in comparison with the results for the NC ( $P<0.001$ ) and BC ( $P<0.001$ ) groups (Fig. 2C and D). No significant difference was observed between the inhibition of *hMSH2* expression in the NC and BC groups ( $P>0.05$ ). Therefore, *hMSH2*-siRNA-1# was used in the subsequent experiments.

*Paclitaxel resistance is reversed by inhibition of hMSH2 expression.* Cell growth inhibition rate curves were constructed for paclitaxel using the following concentration gradient: 0, 1, 2, 4, 8, 16 and 32  $\mu\text{g/ml}$  (Fig. 3A). The inhibitory effect of paclitaxel on cell growth in the EX group was the most obvious. The  $\text{IC}_{50}$  for paclitaxel in the EX group (2.078  $\mu\text{g/ml}$ ) was considerably lower than that in the NC group (13.778  $\mu\text{g/ml}$ ;  $P<0.001$ ) and BC group (14.056  $\mu\text{g/ml}$ ;  $P<0.001$ ; Fig. 3B). No significant difference was observed between the  $\text{IC}_{50}$  values of the NC and BC groups ( $P>0.05$ ).

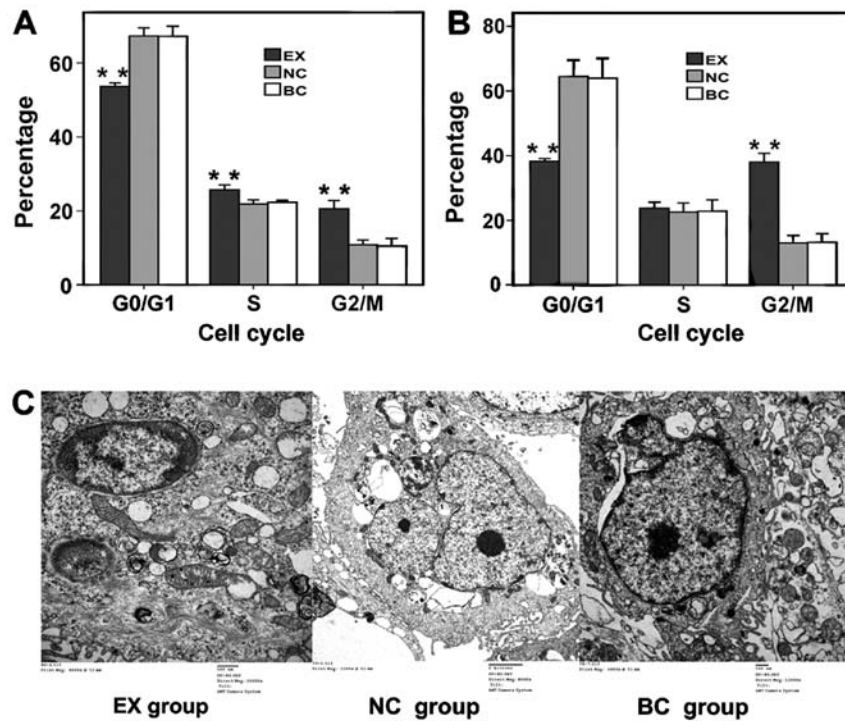


Figure 4. (A) Cell cycle analysis 24 h after paclitaxel (2 μg/ml) treatment in the 3 groups. (B) Cell cycle analysis 48 h after paclitaxel (2 μg/ml) treatment in the 3 groups. (C) Ultrastructural changes in the cells undergoing apoptosis. EX group, chromatin margination, nuclear condensation, and intracytoplasmic vacuoles (scale bar, 500 nm). NC group, cell with nearly normal morphological features, central nuclei and clear nucleoli (scale bar, 2 μm). BC group, mild chromatin pyknosis and marginalized mild swelling of mitochondria (scale bar, 500 nm). EX group, experiment group; NC group, negative control group; BC group, blank control group.

*Apoptosis rate and arrest of the G<sub>2</sub>/M phase of the cell cycle are significantly increased in paclitaxel-treated transfected cells.* The cell cycle progression and apoptosis rate were analyzed after paclitaxel treatment at a concentration of 2 μg/ml. This concentration was selected because it was approximately equivalent to the IC<sub>50</sub> value in the EX group.

The apoptosis rates for the EX group increased with time and were significantly higher at 24 and 48 h (6.45 and 12.46%, respectively) than those for the NC (1.67 and 4.46%, respectively;  $P < 0.001$ ) and BC groups (1.42 and 4.09%, respectively;  $P < 0.001$ ) (Fig. 3C and D). No significant difference was observed between the apoptosis rates for the NC and BC groups ( $P > 0.05$ ). The G<sub>2</sub>/M ratios for the EX group after paclitaxel treatment for 24 and 48 h were significantly higher (20.61 and 38.02%, respectively) than those for the NC (10.84 and 13%, respectively;  $P < 0.001$ ) and BC groups (10.45 and 13.17%, respectively;  $P < 0.001$ ) (Figs. 3E, 4A and B). The S-phase ratios for the EX group after paclitaxel treatment for 24 h were significantly higher (25.70%) than that for the NC (21.85%,  $P < 0.001$ ) and BC groups (22.29%,  $P < 0.001$ ) (Fig. 4A). The G<sub>0</sub>/G<sub>1</sub> ratios for the EX group after paclitaxel treatment for 24 and 48 h were significantly lower (53.69 and 38.23%, respectively) than those for the NC (67.32 and 64.43%, respectively;  $P < 0.001$ ) and BC groups (67.25 and 63.97%, respectively;  $P < 0.001$ ) (Figs. 3E, 4A and B). No significant difference was observed between the cell cycle progression ( $P > 0.05$ ) in the NC and BC groups.

Ultrastructural changes in cells undergoing apoptosis were observed using electron microscopy. Compared with the NC and BC group cells, EX group cells exhibited more visible cell shrinkage, severe chromatin margination, nuclear

condensation, fragmentation, and apoptotic body formation than the control cells. Moreover, the nucleolus disappeared, the mitochondria swelled markedly, mitochondrial cristae disappeared, and other signs of apoptosis appeared. In the NC and BC groups, the nucleus was centrally located in the cells and the nucleolus was clear; the chromatin was pyknotic and marginalized with mild mitochondrial swelling (Fig. 4C).

## Discussion

Our study investigated the relationship between *hMSH2* and paclitaxel resistance in ovarian cancer cell lines for the first time. We found *hMSH2* overexpression in the paclitaxel-resistant cell lines, which was established by exposing OC3 ovarian carcinoma cells to different paclitaxel doses, as well as in the paclitaxel-treated ovarian carcinoma tissues. These findings indicate that *hMSH2* upregulation is related to paclitaxel treatment. We propose the following mechanism to explain this phenomenon: DNA damage to carcinoma cells treated with chemotherapeutic drugs activates *hMSH2* expression. *hMSH2* repairs the drug-induced damage to DNA and prevents tumor cell death.

Subsequent experiments suggested that the poor prognosis of patients with low-differentiated ovarian carcinomas is related to the development of drug resistance. There are many reports concerning the upregulation of *hMSH2* expression in tumors and its correlation with prognosis. For example, Ciavattini *et al* (23) reported that the frequency of *hMSH2* expression in patients with invasive and pre-invasive cervical cancer was higher than that of normal cervical epithelium.

Materna *et al* (24) analyzed 73 ovarian carcinoma samples and found that patients with undetectable *hMSH2* expression experienced higher overall survival rates than those with detectable *hMSH2* expression (81 and 42%, respectively;  $P=0.013$ ). Vageli *et al* (25) reported that patients with lung adenocarcinoma showing increased *hMSH2* expression had poor outcomes compared with those with low *hMSH2* expression. However, contradicting results were obtained for patients with squamous cell carcinoma of the lung. Nadin *et al* (26) found that, at 24 h after chemotherapy, *hMSH1* and *hMSH2* expression in approximately 83% of cisplatin-treated cancer patients with complete responses was higher than the mean value, indicating that the MMR pathway is important for correcting cisplatin-induced DNA damage. Similarly, higher *hMSH2* expression was detected in urinary tract and prostate cancers (27-29).

We further investigated whether we could reverse paclitaxel resistance by inhibiting *hMSH2* expression through RNAi technology. We found that the  $IC_{50}$  of paclitaxel was significantly decreased, and the apoptosis rate and  $G_2/M$  ratios of the cell cycle were significantly increased in paclitaxel treated-transfected cells. The results further confirm that low expression of *hMSH2* could reduce drug resistance, sensitivity to paclitaxel can be restored by knocking down the *hMSH2* gene, and the failure of chemotherapy is associated with the elevated DNA damage repair capacity (13-16,30).

DNA repair systems eliminate the damaged or mismatched nucleotides of DNA and have been confirmed as being closely associated with resistance to chemotherapeutic drugs. DNA repair mechanisms are classified into the following 5 categories according to their basic chemical role in repairing damage (13,31-35). First, direct repair (DR) is a simple way to repair DNA damage.  $O^6$ -methylguanine-DNA methyltransferase (MGMT) is the most important immediate repair enzyme. Wiewrodt *et al* (31) found that MGMT activity of recurrent glioblastomas significantly increased after radiotherapy or a combined treatment with alkylating agents (e.g. temozolomide and chloroethylnitrosoureas). Second, MMR has a mechanism similar to that of DR. Third, base-excision repair, which is the most active DNA repair pathway in mammals, is primarily responsible for the repair of DNA base damage such as base loss and DNA single strand breaks caused by spontaneous hydrolysis, reactive oxygen species, or alkylating agents (32,33). Fourth, nucleotide-excision repair is the major repair process active against larger damages in the DNA of normal cells and is composed of a multi-enzyme DNA repair pathway. One of the most crucial enzymes is the excision repair cross complementing 1 (ERCC1). A high level of ERCC1 expression has been reported in cisplatin-resistant tumors (34-36). Fifth, double-strand break repair (DSBR) comprises 2 sub-pathways: homologous recombination (HR), and non-homologous end joining (NHEJ). Both are mediated by complex pathways that involve a series of components and multi-step reaction processes. The key enzyme in DSBR is Rad51. Studies have found that Rad51 overexpression is an important cause of gefitinib and cisplatin resistance in lung cancer. Knockdown of Rad51 significantly enhanced cell death after cisplatin treatment (37).

DNA repair system provides a potential target for reversing resistance to chemotherapy (38,39). In recent years, many

researchers have synthesized agents that target special DNA repair proteins and have reported that inhibiting DNA damage repair systems may restore the response to chemotherapy in some resistant tumors; combining DNA repair inhibitors with chemotherapeutic drugs can also significantly improve therapy effectiveness. Several clinical trials have been carried out using different DNA damage repair inhibitors that target several enzymes such as PARP, DNA-PK and MGMT (16,36,37,40,41).

Therefore, blocking *hMSH2* expression may be an important new way to treat cancer. However, there are still several barriers to the application of this strategy, since drug resistance is not the result of *hMSH2* expression alone and depends on many other complex pathways and the multiple molecular structure of DNA (8,42). Studies involving the mechanisms underlying the relationship between *hMSH2* and drug resistance should continue in the future.

Our experiments are the first to indicate that the expression of *hMSH2* is upregulated in ovarian carcinoma cell lines and tissues after paclitaxel treatment, and *hMSH2* overexpression is related to paclitaxel resistance and poor prognosis. Inhibition of *hMSH2* expression indicates a new direction in adjuvant therapy for ovarian carcinoma.

#### Acknowledgements

The present study was supported by the National High Technology Research and Development Program of China (grant no. 2006AA02A245).

#### References

- Jemal A, Siegel R, Xu J and Ward E: Cancer statistics, 2010. *CA Cancer J Clin* 60: 277-300, 2010.
- Osterberg L, Levan K, Partheen K, Delle U, Olsson B, Sundfeldt K, *et al*: Specific copy number alterations associated with docetaxel/carboplatin response in ovarian carcinomas. *Anticancer Res* 30: 4451-4458, 2010.
- Takano M, Kudo K, Goto T, Yamamoto K, Kita T and Kikuchi Y: Analyses by comparative genomic hybridization of genes relating with cisplatin-resistance in ovarian cancer. *Hum Cell* 14: 267-271, 2001
- Marcelis CL, van der Putten HW, Tops C, Lutgens LC and Moog U: Chemotherapy resistant ovarian cancer in carriers of an *hMSH2* mutation? *Fam Cancer* 1: 107-109, 2001.
- Honda M, Okuno Y, Hengel SR, *et al*: Mismatch repair protein hMSH2-hMSH6 recognizes mismatches and forms sliding clamps within a D-loop recombination intermediate. *Proc Natl Acad Sci USA* 111: E316-E325, 2014.
- Lynch HT, Lynch PM, Lanspa SJ, Snyder CL, Lynch JF and Boland CR: Review of the Lynch syndrome: history, molecular genetics, screening, differential diagnosis, and medicolegal ramifications. *Clin Genet* 76: 1-18, 2009.
- Masuda K, Banno K, Hirasawa A, *et al*: Relationship of lower uterine segment cancer with Lynch syndrome: A novel case with an *hMLH1* germline mutation. *Oncol Rep* 28: 1537-1543, 2012.
- Yasin SL and Rainbow AJ: A combination of MSH2 DNA mismatch repair deficiency and expression of the SV40 large T antigen results in cisplatin resistance of mouse embryonic fibroblasts. *Int J Oncol* 39: 719-726, 2011.
- Kheirleiseid EA, Miller N, Chang KH, Curran C, Hennessey E, Sheehan M and Kerin MJ: Mismatch repair protein expression in colorectal cancer. *J Gastrointest Oncol* 4: 397-408, 2013.
- Shah SN, Hile SE and Eckert KA: Defective mismatch repair, microsatellite mutation bias, and variability in clinical cancer phenotypes. *Cancer Res* 70: 431-435, 2010.
- Poulogiannis G, Frayling IM and Arends MJ: DNA mismatch repair deficiency in sporadic colorectal cancer and Lynch syndrome. *Histopathology* 56: 167-179, 2010.

12. Kamat N, Khidhir MA, Alashari MM and Rannug U: Microsatellite instability and loss of heterozygosity detected in middle-aged patients with sporadic colon cancer: A retrospective study. *Oncol Lett* 6: 1413-1420, 2013.
13. Chaney SG and Sancar A: DNA repair: enzymatic mechanisms and relevance to drug response. *J Natl Cancer Inst* 88: 1346-1360, 1996.
14. Ding J, Miao ZH, Meng LH and Geng MY: Emerging cancer therapeutic opportunities target DNA-repair systems. *Trends Pharmacol Sci* 27: 338-344, 2006.
15. Fox M and Roberts JJ: Drug resistance and DNA repair. *Cancer Metastasis Rev* 6: 261-281, 1987.
16. Sánchez-Pérez I: DNA repair inhibitors in cancer treatment. *Clin Transl Oncol* 8: 642-646, 2006.
17. Alzoubi K, Khabour O, Khader M, Mhaidat N and Al-Azzam S: Evaluation of vitamin B12 effects on DNA damage induced by paclitaxel. *Drug Chem Toxicol*: Nov 11, 2013 (Epub ahead of print). doi: 10.3109/01480545.2013.851686.
18. Zhang J, Zhao J, Zhang W, *et al*: Establishment of paclitaxel-resistant cell line and the underlying mechanism on drug resistance. *Int J Gynecol Cancer* 22: 1450-1456, 2012.
19. Zhang L, Liu P, Li H and Xue F: Effect of histone deacetylase inhibitors on cell apoptosis and expression of the tumor suppressor genes RUNX3 and ARHI in ovarian tumors. *Mol Med Rep* 7: 1705-1709, 2013.
20. Newell PD, Fricker AD, Roco CA, Chandransu P and Merkel SM: A small-group activity introducing the use and interpretation of BLAST. *J Microbiol Biol Educ* 14: 238-243, 2013.
21. Lin X, Yu Y, Zhao H, Zhang Y, Manela J and Tonetti DA: Overexpression of PKC $\alpha$  is required to impart estradiol inhibition and tamoxifen-resistance in a T47D human breast cancer tumor model. *Carcinogenesis* 27: 1538-1546, 2006.
22. Mi J, Zhang X, Liu Y, Reddy SK, Rabbani ZN, Sullenger BA and Clary BM: NF-kappaB inhibition by an adenovirus expressed aptamer sensitizes TNF-alpha-induced apoptosis. *Biochem Biophys Res Commun* 359: 475-480, 2007.
23. Ciavattini A, Piccioni M, Tranquilli AL, Filosa A, Pieramici T and Goteri G: Immunohistochemical expression of DNA mismatch repair (MMR) system proteins (hMLH1, hMSH2) in cervical preinvasive and invasive lesions. *Pathol Res Pract* 201: 21-25, 2005.
24. Materna V, Surowiak P, Markwitz E, Spaczynski M, Drag-Zalesinska M, Zabel M and Lage H: Expression of factors involved in regulation of DNA mismatch repair- and apoptosis pathways in ovarian cancer patients. *Oncol Rep* 17: 505-516, 2007.
25. Vageli DP, Zaravinos A, Daniil Z, *et al*: hMSH2 and hMLH1 gene expression patterns differ between lung adenocarcinoma and squamous cell carcinoma: correlation with patient survival and response to adjuvant chemotherapy treatment. *Int J Biol Markers* 27: e400-e404, 2013.
26. Nadin SB, Vargas-Roig LM, Drago G, Ibarra J and Ciocca DR: DNA damage and repair in peripheral blood lymphocytes from healthy individuals and cancer patients: a pilot study on the implications in the clinical response to chemotherapy. *Cancer Lett* 239: 84-97, 2006.
27. Leach FS, Hsieh JT, Molberg K, Saboorian MH, McConnell JD and Sagalowsky AI: Expression of the human mismatch repair gene *hMSH2*: a potential marker for urothelial malignancy. *Cancer* 88: 2333-2341, 2000.
28. Prtilo A, Leach FS, Markwalder R, *et al*: Tissue microarray analysis of *hMSH2* expression predicts outcome in men with prostate cancer. *J Urol* 174: 1814-1818, 2005.
29. Li M, Zhang Q, Liu L, Lu W, Wei H, Li RW and Lu S: Expression of the mismatch repair gene hMLH1 is enhanced in non-small cell lung cancer with EGFR mutations. *PLoS One* 8: e78500, 2013.
30. Aebi S, Fink D, Gordon R, Kim HK, Zheng H, Fink JL and Howell SB: Resistance to cytotoxic drugs in DNA mismatch repair-deficient cells. *Clin Cancer Res* 3: 1763-1777, 1997.
31. Wiewrodt D, Nagel G, Dreimüller N, Hundsberger T, Pernecky A and Kaina B: MGMT in primary and recurrent human glioblastomas after radiation and chemotherapy and comparison with p53 status and clinical outcome. *Int J Cancer* 122: 1391-1399, 2008.
32. Cadet J, Douki T, Gasparutto D and Ravanat JL: Oxidative damage to DNA: formation, measurement and biochemical features. *Mutat Res* 531: 5-23, 2003.
33. Gurubhagavatula S, Liu G, Park S, *et al*: XPD and XRCC1 genetic polymorphisms are prognostic factors in advanced non-small-cell lung cancer patients treated with platinum chemotherapy. *J Clin Oncol* 22: 2594-2601, 2004.
34. Chen HY, Shao CJ, Chen FR, Kwan AL and Chen ZP: Role of ERCC1 promoter hypermethylation in drug resistance to cisplatin in human gliomas. *Int J Cancer* 126: 1944-1954, 2010.
35. Steffensen KD, Smoter M, Waldstrøm M, *et al*: Resistance to first line platinum paclitaxel chemotherapy in serous epithelial ovarian cancer: The prediction value of ERCC1 and Tau expression. *Int J Oncol* 44: 1736-1744, 2014.
36. Li QQ, Lee RX, Liang H, Wang G, Li JM, Zhong Y and Reed E:  $\beta$ -Elemene enhances susceptibility to cisplatin in resistant ovarian carcinoma cells via downregulation of ERCC-1 and XIAP and inactivation of JNK. *Int J Oncol* 43: 721-728, 2013.
37. Ko JC, Ciou SC, Cheng CM, *et al*: Involvement of Rad51 in cytotoxicity induced by epidermal growth factor receptor inhibitor (gefitinib, Iressa<sup>®</sup>) and chemotherapeutic agents in human lung cancer cells. *Carcinogenesis* 29: 1448-1458, 2008.
38. Zhu Y, Hu J, Hu Y and Liu W: Targeting DNA repair pathways: a novel approach to reduce cancer therapeutic resistance. *Cancer Treat Rev* 35: 590-596, 2009.
39. Curtin N: Therapeutic potential of drugs to modulate DNA repair in cancer. *Expert Opin Ther Targets* 11: 783-799, 2007.
40. Mohammed MZ, Vyjayanti VN, Laughton CA, *et al*: Development and evaluation of human AP endonuclease inhibitors in melanoma and glioma cell lines. *Br J Cancer* 104: 653-663, 2011.
41. Rodon J, Iniesta MD and Papadopoulos K: Development of PARP inhibitors in oncology. *Expert Opin Investig Drugs* 18: 31-43, 2009.
42. Lenglet G and David-Cordonnier MH: DNA-destabilizing agents as an alternative approach for targeting DNA: mechanisms of action and cellular consequences. *J Nucleic Acids* 2010: 290935, 2010.